



## Microstructure, microsegregation pattern and the formation of B2 phase in directionally solidified Ti–46Al–8Nb alloy

Guohuai Liu, Xinzhong Li\*, Yanqing Su, Dongmei Liu, Jingjie Guo, Hengzhi Fu

School of Materials Science and Engineering, Harbin Institute of Technology, P.O. Box 434, Harbin 150001, PR China

### ARTICLE INFO

#### Article history:

Received 9 February 2012  
Received in revised form 4 July 2012  
Accepted 6 July 2012  
Available online 16 July 2012

#### Keywords:

TiAl-based alloy  
Directional solidification  
Microstructure  
Phase transformation

### ABSTRACT

Bridgman type directional solidification experiments were conducted for Ti–46Al–8Nb alloy in a wide range of growth rates (1–70  $\mu\text{m/s}$ ). The microstructure, microsegregation and the formation of B2 phase were investigated. Nearly planar and shallow cellular growths of primary  $\beta$  phase were observed at the growth rates of 1 and 2  $\mu\text{m/s}$  respectively, and a fully  $\alpha_2/\gamma$  lamellar structure was formed finally. The growth rates of (2–5  $\mu\text{m/s}$ ) and ( $\geq 5$   $\mu\text{m/s}$ ) resulted in the transient cellular-dendritic and regular dendritic growth respectively, which were accompanied with sequent peritectic reaction resulting from the shift of  $L + \beta \rightarrow \beta$  transus line to lower aluminum content with increasing growth rate. Peritectic reaction promoted niobium enriched in the core of dendrites and the formation of B2 phase, which mainly was due to the stabilization of  $\beta$  phase during the  $\beta \rightarrow \alpha$  transformation and precipitated from  $\alpha$  lamellae through the  $\alpha + \gamma \rightarrow \alpha_2 + \gamma + \text{B2}$  transformation. The final microstructure was composed of  $\alpha_2/\gamma$  lamellar structure and B2 phase.

© 2012 Elsevier B.V. All rights reserved.

### 1. Introduction

TiAl-based alloys have attracted much attention as potential candidate for high temperature structural application for its excellent low density, high specific modulus and creep resistance [1–5]. However, the practical use of these alloys still needs the improvement in properties, such as room temperature ductility, high temperature strength and oxidation resistance above 800 °C. Alloying element Nb is added to improve high temperature resistance, lamellar structure stability and oxidation resistance [6,7]. Especially, Ti–46Al–8Nb (at.%) intermetallic alloy developed within the pan-European IMPRESS project is both lightweight and creep resistant to high temperatures ( $\sim 800$  °C), so being one of the advanced materials for turbines of aircraft engines and gas-burning power-generation plants [8,9]. However, high Nb addition changes the TiAl phase diagram greatly, leading to the solidification behavior different from binary TiAl alloys [10,11]. The complex solidification path and also subsequent solid-state transformation limit understanding of microstructure development in Nb-additional TiAl alloys. Directional solidification is an appropriate technique to research solidification behavior of alloy under defined solidification conditions [12]. Ding et al. [13] had showed that the peritectic

reaction could be found at a lower growth rate in directionally solidified Ti–45Al–8Nb (at.%) alloy. While Gabalcová et al. [14] showed that the studied Ti–46Al–8Nb alloy solidified through  $\beta$ -phase without any evidence of peritectic reaction within a wide range of growth rates during directional solidification. The solidification pathway can be greatly affected by the microsegregation. Therefore, further study on the solidification pathways, microsegregation and microstructure evolution by the directional solidification is still needed.

In addition, the addition of the  $\beta$ -stabilizers such as Nb usually leads to stabilization of the  $\beta$  phase at lower temperature in the form of ordered B2 phase, which could greatly affect the mechanical properties of the alloys [13,15,16]. Various morphologies and origins of the B2 phase in high Nb containing TiAl-based alloys have been reported by several authors [15,17,18]. Chen et al. [17] had observed that both the  $\beta$ -segregation from the  $\beta \rightarrow \alpha$  transformation and the  $\alpha$ -segregation during the  $\alpha \rightarrow \alpha + \gamma + \beta$  transformation could be as the origins of the B2 phase in the cast Ti–45Al–(8–9) Nb–(W, B, Y) alloy. A recent study by Zollinger et al. [18] had shown that the B2 phase only formed during the  $\beta \rightarrow \alpha$  transformation in directional solidified Ti–46Al–8Nb alloy. However, Yuyong Chen et al. [15] had showed that B2 precipitate largely formed via the transformation of  $\alpha + \gamma \rightarrow \alpha_2 + \gamma + \beta$  transformation during aging of Ti–45Al–2Nb–1.5V–1Mo–0.3Y alloy. Up to now, the formation of B2 phase depends on the solidification behavior and corresponding microsegregation pattern greatly, which is not yet fully understood.

\* Corresponding author. Address: School of Materials Science and Engineering, Harbin Institute of Technology, 92 Xidazhi Street, Harbin 150001, PR China. Tel.: +86 451 86418815.

E-mail address: [hitlxz@126.com](mailto:hitlxz@126.com) (X. Li).

The aim of this study was to determine the microstructure, microsegregation and the formation of B2 phase by quenching during directional solidification of Ti–46Al–8Nb (at.%) alloy. The phase transition path, the detailed microstructure evolution and the microsegregation pattern were investigated at the growth rates ranging from 1 to 70  $\mu\text{m/s}$ . A particular interest was the effect of microsegregation on phase transition pattern involving both the solidification path and the formation of B2 phase.

## 2. Experimental procedures

The intermetallic Ti–46Al–8Nb alloy with an actual composition of Ti–46.3Al–7.6Nb (at.%) was supplied in the form of cast cylindrical ingot, which was fabricated by the induction skull melting (ISM) under argon atmosphere. The samples were machined to rods with 3 mm diameter and 100 mm in length from the ingot by a spark machining and placed into the alumina crucible, which had an yttria mould isolating the alloy from the crucible described in detail in our previous work [19,20]. The Bridgman type apparatus was employed to produce the directionally solidified bar under the protection of the high-purity argon. Each sample was heated to 1790 °C and held for 30 min before directional solidification, and then was directionally solidified with growth rates from 1 to 70  $\mu\text{m/s}$ . After growing 40 mm during directional solidification, the sample was quenched into the liquid Ga–In–Sn alloy to restore the solid–liquid interface. The temperature gradient was measured by W/Re thermocouples that were placed near the outside surface of the alumina tubes, as was illustrated in Ref. [21]. The temperature gradient close to the solid–liquid interface was measured to be approximately 25 K/mm.

After directional solidification, the longitudinal and transverse sections of the specimens were cut. Microstructure analysis was performed by optical microscopy (OM), scanning electron microscopy (SEM) equipped with an energy dispersive spectrometer (EDS) and transmission electron microscopy (TEM). OM and SEM samples were prepared using standard metallographic techniques and etched with a solution of 10 ml HF–10 ml  $\text{HNO}_3$ –180 ml  $\text{H}_2\text{O}$ . The different phases present in the microstructure were discriminated based on their contrast on Back-scattered Electron (BSE) images and the component distribution was determined by EDS. The samples for TEM were mechanically thinned to a thickness of about 40  $\mu\text{m}$ . Thinning was electropolished in a solution. Lamellar structure, individual crystallographic orientation and B2 phase at higher magnification were determined by computerized image analysis.

## 3. Results and discussion

### 3.1. Structure of DS ingots

#### 3.1.1. The morphology of the quenching interface

Fig. 1 shows the morphologies of the quenching solid–liquid interface (a–g) and some typical peritectic interface (h–i) at the selected growth rates in directionally solidified Ti–46Al–8Nb alloy. Cubic  $\beta$  is easily found to be the primary solidification phase in this alloy by noting that the secondary dendritic arms are orthogonal to the primary arms, as shown in Fig. 1(e–g). Nearly planar and shallow cellular growths are observed at the growth rates of 1 and 2  $\mu\text{m/s}$  respectively, as shown in Fig. 1(a) and (b). Transient cellular-dendritic growth is found at the growth rates ranging from 3 to 5  $\mu\text{m/s}$ . The higher growth rates ( $\geq 5 \mu\text{m/s}$ ) result in a regular dendritic growth.

As shown in Fig. 1(h) and (i), the typical peritectic reaction can be observed at high growth rates ( $\geq 3 \mu\text{m/s}$ ), and the peritectic reaction interface is gradually away from the quenching interface with the increase of the growth rate, as shown in Fig. 1(c–g). The growth of primary  $\beta$  phase leading to the solute segregation in the interdendritic region promotes the occurrence of the peritectic  $\alpha$  phase. After the nucleate of peritectic  $\alpha$  phase adhering to primary  $\beta$  phase, the sequent growth of  $\alpha$  phase needs the solute diffusion between the liquid and  $\beta$  phase whose driving force depends on the local concentrations difference of  $\alpha$  phase, i.e. the solid solubility limit [22]. Due to the low diffusion rate in solid phase relative to the cooling rate it is difficult to conduct a complete peritectic reaction, especially at a high growth rate corresponding to a high cooling rate. So retained frame of  $\beta$  dendrites in the core of dendrites can be observed clearly in Fig. 1(h) and (i).

The critical growth rate of the studied alloy maintaining a planar interface could be determined according to relationship in the form:

$$\frac{G_L}{V} \geq \frac{\Delta T}{D_L} \quad (1)$$

where  $D_L$  is the diffusion coefficient in the liquid ( $D_L = 2.8 \times 10^{-9} \text{ m}^2 \text{ s}^{-1}$  in the studied alloy),  $\Delta T$  is the freezing interval about 65 K for Ti–46Al–8Nb (at.%) alloy obtained by the thermal analysis (DTA) [14], and  $G_L$  is the temperature gradient in the liquid about 25 K/mm in present. Then the critical growth rate of 1.08  $\mu\text{m/s}$  can be obtained, which is bigger than the present experimental result ( $V_c = 0.664 \mu\text{m/s}$ ) in directionally solidified Ti–46Al–2W–0.5Si (at.%) alloy obtained by Lapin et al. The discrepancy of the critical growth rate can be attributed to the change of the solidification range and the temperature gradient.

Fig. 2 shows the effect of the growth rates on the primary dendritic spacing. During the cellular-dendritic growth of primary  $\beta$  phase at the low growth rates ( $1 \mu\text{m/s} < V < 5 \mu\text{m/s}$ ), the primary spacing increases with increasing growth rate. It can be attributed to the occurrence of the secondary dendrite inhibiting the growth of the primary dendrite, then promoting the bigger primary dendritic spacing. During the growth of regular dendrites at higher growth rates ( $\geq 5 \mu\text{m/s}$ ), the spacing decreases proportionally with increasing growth rate. The relationship between the primary dendritic spacing  $\lambda$  and the higher growth rate  $V$  ( $\geq 5 \mu\text{m/s}$ ) is obtained by using linear regression analysis. The result is given as:

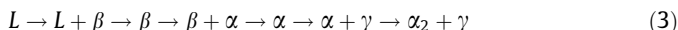
$$\lambda = 719.88V^{-0.21} \quad (2)$$

Taking account of a constant temperature gradient, the exponent of 0.21 in Eq. (2) is comparable with that of 0.25 resulting from the models of Kurz and Fisher [23] and that of 0.24 reported by Lapin et al. [24] for DS Ti–46Al–2W–0.5Si (at.%) alloy, but lower than that of 0.31 for a binary Ti–49Al (at.%) alloy [19] and that of 0.47 for DS Ti–46Al–0.5W–0.5Si (at.%) alloy [25] reported by Jianglei Fan et al. The discrepancy of these values could be attributed to the difference of the composition of alloys and solidification conditions.

#### 3.1.2. Phase transition path

Fig. 3 shows the macro- and microstructures of interest at the growth rates of 2 and 30  $\mu\text{m/s}$  after quenching during directional solidification. Quenching quickly allows freezing-in the high temperature phases for subsequent analysis.

At the growth rate of 2  $\mu\text{m/s}$ , the shallow cellular growth of single primary  $\beta$  phase is observed at the quenching solid–liquid interface, as shown in Fig. 3(c). After a series of phase transformation, the final microstructure consists of the lamellar structure of  $\alpha_2(\text{Ti}_3\text{Al})$  and  $\gamma$  (TiAl). The lamellar structure has a 45° orientation to the growth direction, which also indicates that the  $\beta$  phase is as the primary phase, as shown in Fig. 3(b). From this point of view, experimentally determined phase transition path at the growth rate of 2  $\mu\text{m/s}$  could be described as follow:



At the growth rate of 30  $\mu\text{m/s}$ , the dendritic growth of primary  $\beta$  phase is observed at the quenching solid–liquid interface. Particularly, a liquid,  $\alpha$  and  $\beta$  mixing zone is found at the positions behind the  $\beta$  phase tips compared to the microstructure at the growth rate of 2  $\mu\text{m/s}$ , where the peritectic  $\alpha$  phase envelopes the primary phase  $\beta$  firstly by nucleation. Then, the dissolution of primary  $\beta$  and growth of peritectic  $\alpha$  happen near the trijunction, as shown in Fig. 3(d). As the decrease of the temperature, the final microstructure is observed consisted of three phases namely  $\gamma$  (TiAl),  $\alpha_2$  ( $\text{Ti}_3\text{Al}$ ) and B2 phase. The bright B2 phase can be observed

Download English Version:

<https://daneshyari.com/en/article/1615455>

Download Persian Version:

<https://daneshyari.com/article/1615455>

[Daneshyari.com](https://daneshyari.com)